J|A|C|S
ARTICLES
Published on Web 01/11/2005

# Structure, Assembly, and Topology of the G185R Mutant of the Fourth Transmembrane Domain of Divalent Metal Transporter

Fei Li, Hongyan Li, Lihong Hu, Miufan Kwan, Guanhua Chen, Qing-Yu He,* and Hongzhe Sun*

*Contribution from the Department of Chemistry and Open Laboratory of Chemical Biology, The University of Hong Kong, Pokfulam Road, Hong Kong, People's Republic of China*

Received May 15, 2004; E-mail: hsun@hkucc.hku.hk

***Abstract:*** The mammalian iron transporter, divalent metal transporter (DMT1), is a 12-transmembrane domain integral protein, responsible for dietary iron uptake in the duodenum and iron acquisition from transferrin in peripheral tissues. Two disease-causing mutants in animals have been found and attributed to the same missense mutation (G185R), which occurs within the putative transmembrane domain 4 (TM4) of DMT1. We have characterized a synthetic 24-mer peptide, corresponding to the sequence of the TM4 of DMT1 with G185R mutation using circular dichroism (CD) and NMR spectroscopy and show that the G185R peptide assumes mainly α-helical conformations in various membrane-mimetic environments. Solution structures derived from NMR and molecular dynamics/simulated annealing calculations demonstrate that the peptide exhibits a highly defined α-helix in its middle portion, flanked by a highly flexible N-terminus and a relatively ordered C-terminus. Both the folding and location of the C-terminus in SDS micelles are regulated by pH values. Paramagnetic broadening on peptide NMR signals by spin-labeled 5- and 16-doxylstearic acids and $Mn^{2+}$ ion suggests that both the N-terminus and the helical region of the peptide are embedded in SDS micelles. Surprisingly, self-association of the peptides for both the wild type and the G185R mutant studied by CD, electrospray ionization mass spectrometry, and NMR diffusion-ordered spectroscopy demonstrated that mutation of the Gly185 to a bulky and positively charged arginine causes a different self-assembly of the peptide, e.g., from a trimer to a hexamer, which implies that the quaternary structure of integral DMT1 may be crucial for its function in vivo.

## Introduction

Divalent metal transporter 1 (DMT1), also known as DCT1 and Nramp2 (natural resistance-associated macrophage protein 2), mediates apical iron uptake into the duodenal enterocytes and also transfers iron from the endosome into the cytosol after cellular uptake via the transferrin receptor.[1−4] It consists of 561 amino acids with 12 putative transmembrane domains, and is ubiquitously expressed, most notably in the proximal duodenum.[1] Functional studies of *Xenopus laevis* oocytes and cultured mammal cells have demonstrated that DMT1 transports not only $Fe^{2+}$ but also a broad range of other divalent metal ions, such as $Zn^{2+}$, $Mn^{2+}$, $Co^{2+}$, $Cd^{2+}$, $Cu^{2+}$, $Ni^{2+}$, and $Pb^{2+}$.[1,5] The transport has been shown to be pH-dependent and coupled to proton symport.[1,6] The transmembrane domain 4 (TM4) in DMT1 is involved in two naturally occurring disease-causing mutants in *mk* mice and *Belgrade* rats, which exhibit severe microcytic anemia associated with defects in impaired iron absorption by intestinal cells and in erythroid iron use.[7] Both animals carry an identical mutation in DMT1, i.e., a mutation from a glycine to an arginine (G185R) within the putative transmembrane domain 4, which is highly conserved among Nramp family proteins.[2,8] The G185R mutation of murine DMT1 causes a near-total loss of the capacity for iron transport in transfected HEK293T cells, while overexpression of the wild type (but not the G185R mutant) of DMT1 in HEK293T cells stimulates cellular iron uptake.[9] Similar results have been obtained from mutagenesis studies of DMT1 in yeast and mammalian cells, where the introduction of a bulky and charged residue (G185R) in the TM4 caused a partial or complete loss of the function of DMT1.[10]

DMT1 plays an important role in maintaining intracellular iron homeostasis; however, the mechanism remains poorly

(1) Gunshin, H.; Mackenzie, B.; Berher, U. V.; Gunshin, Y.; Romero, M. F.; Boron, W. F.; Nussberger, S.; Gollan, J. L.; Hediger, M. A. *Nature* **1997**, *388*, 482−488.
(2) Fleming, M. D.; Trenor, C. C., III; Su, M. A.; Foernzler, D.; Beier, D. R.; Dietrich, W. F.; Andrews, N. C. *Nat. Genet.* **1997**, *16*, 383−386.
(3) Canonne-Hergaux, F.; Gruenheid, S.; Ponka, P.; Gros, P. *Blood* **1999**, *93*, 4406−4417.
(4) Tabuchi, M.; Yoshimori, T.; Yamaguchi, K.; Yoshida, T.; Kishi, F. *J. Biol. Chem.* **2000**, *275*, 22220−22228.
(5) Picard, V.; Govoni, G.; Jabado, N.; Gros, P. *J. Biol. Chem.* **2000**, *275*, 35738−35745.
(6) Okubo, M.; Yamada, K.; Hosoyamada, M.; Shibasaki, T.; Endou, H. *Toxicol. Appl. Pharmacol.* **2003**, *187*, 162−167.
(7) Oates, P. S.; Morgan, E. H. *Am. J. Physiol.* **1996**, *270*, G826−G832.
(8) Fleming, M. D.; Romero, M. A.; Su, M. A.; Garrick, L. M.; Garrick, M. D.; Andrews, N. C. *Proc. Natl. Acad. Sci. U.S.A.* **1998**, *95*, 1148−1153.
(9) Su, M. A.; Trenor, C. C., III; Fleming, J. C.; Fleming, M. D.; Andrews, N. C. *Blood* **1998**, *92*, 2157−2163.
(10) Tseung, S. L. L.; Govoni, G.; Forbes, J.; Gros, P. *Blood* **2003**, *101*, 3699−3707.


**10.1021/ja047148t CCC: $30.25** 

understood. Three-dimensional structural study of DMT1 in membrane-like environments is a key step toward understanding its biological function. Unfortunately, there has been little success in the preparation of high-quality three-dimensional crystals of membrane proteins, and the determination of their structures in solution by multidimensional NMR spectroscopy has been hampered by the large size and slow reorientation rate of proteins complexed with lipid, which severely broaden the NMR signals.[11] However, model peptides, corresponding to the sequence of possible functional domains, have proved to be very useful in providing qualitative structural information and in guiding complete structure determination for integral proteins.[12,13] For example, 3D structure models of 12-transmembrane domain lactose permease have been derived without using crystals, on the basis of its transmembrane topology, secondary structure, and numerous interhelical contacts.[14]

We have recently characterized the structures and topology of a peptide, corresponding to the sequence of the transmembrane domain 4 of rat DMT1 (DMT1-TM4) in various membrane-mimicking environments.[15,16] In the present study we use both circular dichroism (CD) spectropolarimetry and NMR spectroscopy to characterize the secondary and three-dimensional structures of a synthetic G185R peptide in TFE and SDS micelles at various pH values. The orientation of the peptide in SDS micelles at different pH values is investigated by the aid of spin-labeled doxylstearic acids and paramagnetic metal ions. The self-association state of the G185R peptide is investigated by CD, electrospray ionization mass spectrometry (ESI-MS), and diffusion-ordered spectroscopy. The results for the mutant peptide are compared with those obtained for the wild-type DMT1-TM4.

## Results

**Circular Dichroism Studies.** The G185R peptide is insoluble in water and a range of organic solvents. Membrane-mimetic environments were therefore chosen to solubilize the peptide and to mimic biological membranes. The secondary structure of the G185R peptide in both SDS micelles and TFE was probed by far-UV CD spectroscopy (Figure 1). The CD spectra were characterized by two negative minima at 208 and 222 nm, and one positive maximum at 194 nm, indicative of the presence of a predominating α-helical conformation. Similar spectra were observed in the presence of HFIP and DPC micelles (data not shown). The CD spectra were deconvoluted using the CDPro software.[57] The α-helical content for the G185R peptide was estimated at ca. 64% in TFE, and ca. 52% at pH 4.0−5.5 and ca. 43% at pH 6.0−7.4 in SDS micelles.

**NMR Assignment and Secondary Structure Estimation.** NMR sequence-specific resonance assignments were carried out using the conventional approach,[17] utilizing TOCSY and NOESY spectra. Spin systems were initially identified using

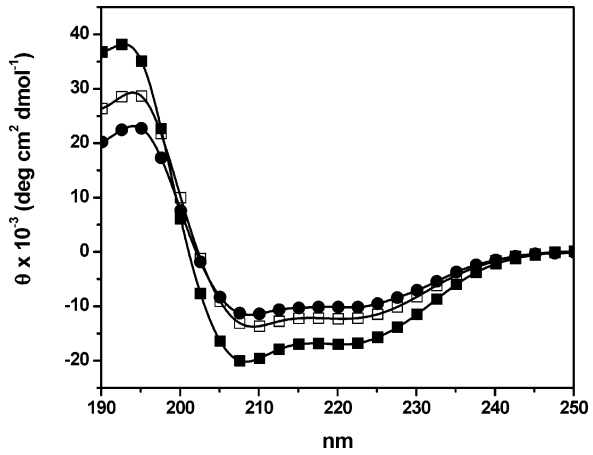


***Figure 1.*** CD spectra of the G185R peptide (20 μM) in TFE (■) and 10 mM SDS at pH 5.5 (□) and 7.4 (●).

TOCSY spectra, and an NOESY spectrum was then used to identify sequential backbone connectivities (Figure 2A,C). The observed medium-range NOEs, e.g., $d_{\alpha N}(i, i + 3)$, $d_{\alpha\beta}(i, i + 3)$, and $d_{\alpha N}(i, i + 4)$, suggest an α-helical structure of the peptide from Tyr5 to Asp22 in TFE (Figure 2B), and Val8 to Phe20 in SDS at pH 6.0 (Figure 2D). Similar results were obtained from predictions using the chemical shift index (CSI)[18] of the $H^{\alpha}$ atoms (Figure 2B,D). Unfortunately, a further estimation of the peptide secondary structure from the backbone *J*-coupling constants ($^3J_{H^N-H^{\alpha}}$) could not be obtained from standard DQF-COSY experiments due to severe line broadening that occurred in both TFE and micellar environments.

The NOESY spectra of the G185R peptide in SDS micelles at pH 7.4 and 4.0 were also recorded and assigned. Similarly, the peptide was found to exhibit an α-helical span from Val8 to Phe20 at pH 6.0 and a similar conformation at pH 7.4, on the basis of both NOE connectivities and the CSI (data not shown). At pH 4.0, however, the helical segment of the peptide extended more toward the C-terminus, spanning from Val8 to Asp22.

**Three-Dimensional Structures of G185R Peptide in TFE and SDS Micelles.** All distance constraints determined experimentally were included in the structural calculation of the G185R peptide, both in TFE and in the SDS micelles. The evaluated structural statistics for the 20 best-converging energy-minimizing structures are summarized in Table 1.

The structure of the G185R peptide in TFE was calculated using 233 nonredundant distance constraints resulting from 355 NOE cross-peaks in the NOESY spectrum with a mixing time of 200 ms. The structural calculation resulted in an average target function of 0.13 Å for the 20 best-fit conformers, with a mean energy of −1000.6 kcal·mol$^{-1}$ calculated from AMBER7. The segment from Val8 to Asp22 was well defined, with root-mean-square deviations to the mean structure of 0.53 Å for backbone heavy atoms and 1.25 Å for all heavy atoms. Ramachandran analysis for the defined segment showed that 73.3% of the backbone dihedral angles fell in the most favored region and the remainder were in the additional allowed region.

The superposition of the 20 best-converging energy-minimizing structures is shown in Figure 3. The generated conformers had well-defined structures which were predominantly α-helical

(11) Opella, S. J.; McDonnell, P. A. In *NMR of Proteins*; Clore, G. M., Gronenborn, A. M., Eds.; CRC: Boca Raton, FL, 1993.
(12) Xie, H.; Ding, F. X.; Schreiber, D.; Eng, G.; Liu, S. F.; Arshava, B.; Arevalo, E.; Becker, J. M.; Naider, F. *Biochemistry* **2000**, *39*, 15462−15474.
(13) Ding, F. X.; Xie, H.; Arshava, B.; Becker, J. F.; Naider, F. *Biochemistry* **2001**, *40*, 8945−8954.
(14) Sorgen, P. L.; Hu, Y.; Guan, L.; Kaback, H. R.; Girvin, M. E. *Proc. Natl. Acad. Sci. U.S.A.* **2002**, *99*, 14037−14040.
(15) Li, H. Y.; Li, F.; Sun, H.; Qian, Z. M. *Biochem. J.* **2003**, *372*, 757−766.
(16) Li, H. Y.; Li, F.; Qian, Z. M.; Sun, H. *Eur. J. Biochem.* **2004**, *271*, 1938−1951.
(17) Wüthrich, K. *NMR of Proteins and Nucleic Acids*; Wiley: New York, 1986.
(18) Wishart, D. S.; Sykes, B. D.; Richards, F. M. *Biochemistry* **1992**, *31*, 1647−1651.

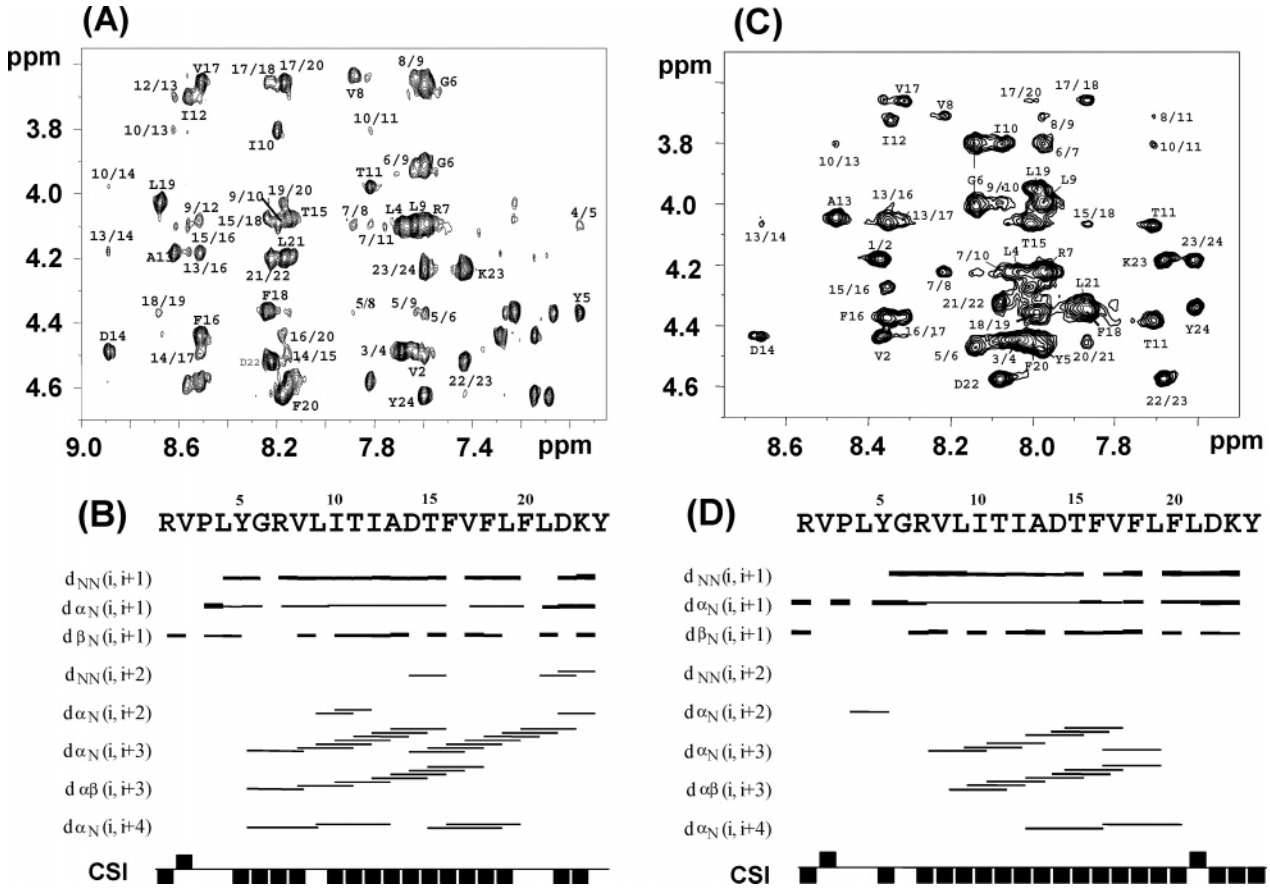


***Figure 2.*** $H^N-H^\alpha$ regions of the 600 MHz NOESY spectra of the G185R peptide (2 mM) with assignments and key NOEs labeled, NOE connectivities, and chemical shift index summarized in TFE at 25 °C (A, B), and in 300 mM SDS-$d_{25}$ at pH 6.0 and 25 °C (C, D).

***Table 1.*** Structural Statistics of the G185R Peptide in SDS (pH 6) and TFE at 25 °C for the 20 Best-Converging Energy-Minimizing NMR Structures

| structural statistics | SDS | TFE |
|---|---|---|
| total number of nonredundant distance constraints | 245 | 233 |
| number of intraresidual distance constraints | 110 | 115 |
| number of sequential distance constraints | 92 | 57 |
| number of medium-range ($\|i-j\| \leq 4$) distance constraints | 43 | 61 |
| number of long-range ($\|i-j\| > 4$) distance constraints | 0 | 0 |
| number of distance constraint violations >0.3 Å (per structure) | 0 | 0 |
| average number of distance restraint violations >0.2 Å (per structure) | 0 | 0 |
| average sum of distance restraint violations (Å) (per residue) | 1.11 ± 0.24 | 1.13 ± 0.23 |
| average maximum distance restraint violation (Å) | 0.17 ± 0.03 | 0.18 ± 0.05 |
| average target function (Å$^2$) | 0.17 ± 0.03 | 0.13 ± 0.03 |
| RMSD from the mean structure (Å) | | |
| all residues | | |
| backbone atoms | 2.72 ± 0.83 | 1.46 ± 0.45 |
| all heavy atoms | 3.92 ± 0.86 | 2.63 ± 0.58 |
| residues 9−20 in SDS and 8−22 in TFE | | |
| backbone atoms | 0.38 ± 0.14 | 0.53 ± 0.18 |
| all heavy atoms | 1.14 ± 0.28 | 1.25 ± 0.27 |
| AMBER energy (kcal·mol$^{-1}$) | −1042.5 ± 9.2 | −1000.6 ± 33.6 |
| Ramachandran statistics from PROCHECK-NMR[a] | | |
| residues in allowed region, % | 100 | 100 |
| residues in disallowed region, % | 0 | 0 |

[a] The program PROCHECK-NMR was used to check the residue regions from 9 to 20 for the peptide in SDS micelles and from 8 to 22 for the peptide in TFE.

from the residues Val8 to Asp22. The N-terminus from Arg1 to Arg7 was flexible and poorly defined, consistent with few medium-range NOE connectivities. In the α-helical region (Val8−Asp22), the $H_{i+4}{}^N-CO_i$ hydrogen bonds were found in most of the structures, and the angular order parameters of $\psi$ and $\phi$ were larger than 0.97, except for the $\phi$ of Phe20 (0.89). On the basis of the prediction from the NOE connectivities and secondary chemical shift analysis, the fragment of Tyr5−Arg7 should also be included in the α-helical region. However, the NOE constraints involved in this fragment were not sufficient to repeatedly produce helical dihedral angles. Consequently, relatively lower dihedral angle order parameter values (from

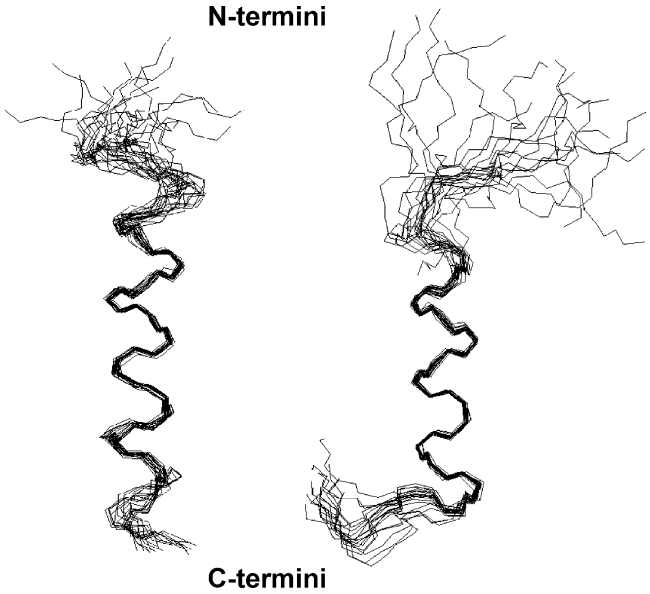


***Figure 3.*** NMR solution structures of the G185R peptide in TFE and SDS micelles: backbone atoms of the 20 best-converging energy-minimizing structures in TFE (left) and in SDS at pH 6.0 (right) with superimpositions over the backbone atoms of residues Val8−Asp22 and Leu9−Phe20, respectively.

0.63 to 0.98) were obtained for Tyr5−Arg7. The Pro3 was in a *trans* conformation, characterized by an observed strong NOE between the $H^{\alpha}$ of Val2 and the $H^{\delta}$ of Pro3.

For the G185R peptide in SDS micelles at pH 6.0, 245 meaningful distance constraints were produced from a total of 362 NOE cross-peaks in the NOESY spectrum with a mixing time of 200 ms. The mean target function of 0.17 Å was obtained for the 20 best-converging conformers, and the mean AMBER energy was calculated to be $-1042.5$ kcal·mol$^{-1}$ after energy minimization. The superposition over the backbone heavy atoms of residues Leu9−Phe20 resulted in RMSDs to the mean structure of 0.38 Å for heavy backbone atoms and 1.14 Å for all heavy atoms (Figure 3). Ramachandran analysis for the defined segment showed that 92.5% of the backbone dihedral angles dropped in the most favored region, while the remainder were in the additional allowed region.

The G185R peptide formed a well-defined α-helix from residue Leu9 to residue Phe20 in SDS micelles at pH 6.0 (Figure 4). Right after the helix, a turn located at Leu21 was identified. This turn forced the backbone of the C-terminal residues to orient nearly perpendicular to the helical axis (Figure 4). In contrast, the N-terminal residues displayed a poorly converged extended conformation. The tertiary structure calculation is in good agreement with the suggestions based on NOE patterns and chemical shift analysis. In most of the structures, $H_{i+4}{}^{N}-CO_i$ hydrogen bonds were found in the helical fragment from residue Val8 to residue Leu19.

The structures of the G185R peptide in SDS micelles at both pH 7.4 and 4.0 were subsequently calculated using methods similar to those described above. To highlight the structural differences at various pH values, the backbone structures of the 20 best-converged energy-minimized conformers at these pH values have been overlaid (Figure 4A). The peptide exhibited similar helical spanning regions (Ile10−Phe20 at pH 7.4 versus Leu9−Phe20 at pH 6.0). Both helices ended at Phe20, and were followed by a turn located at Leu21. However, the α-helix was three residues longer at pH 4.0 (Val8−Asp22) than at pH 6.0 (Leu9−Phe20), consistent with the results of our CD experiments. The extension of the helix sprang largely from the C-terminus (Figure 4A). In particular, the side chain of Phe20 was observed to orientate differently at different pH values. The phenyl rings of Phe16 and Phe20 were more or less parallel at pH 4.0, but were perpendicular to each other at pH 6.0 and 7.4. The N-terminus was disordered and poorly defined at all pH values studied. Distribution of the side chains of the mean structure for the G185R peptide in SDS micelles at pH 6.0 (Figure 4B) illustrated an amphipathetic characteristic. Hydrophilic residues Arg7, Thr11, Asp14, Thr15, and Asp22 lay on one side of the helix, while hydrophobic residues occupied the opposite side. Such an arrangement is likely to provide a basis for the formation of channel architecture.

**Self-Association.** To determine whether the helical structure in the G185R peptide was unimolecular or resulted from aggregation, CD spectra were measured versus concentration. The dependence of the molar residue ellipticity ($\theta$) at 222 nm ($\theta_{222}$) for both the wild-type DMT1-TM4 and the G185R peptides in HFIP on peptide concentrations is shown in Figure 5. The $\theta_{222}$ increased with peptide concentrations, demonstrating that there were intermolecular interactions.[19,20] However, the wild-type and G185R mutant peptides exhibited different changing patterns, indicative of potential different aggregation features. An attempt to study the aggregation behavior in SDS micelles via a similar method was unsuccessful since the structure of the peptide depends on both the SDS concentration and the ratio of SDS to the peptide.

It has been shown previously that the ESI-MS technique is applicable for investigation of self-association of peptides, even in an aqueous TFE system.[21,22] However, the aggregation number of peptides cannot be simply identified by the singly charged molecular ions, due to the upper limit of the working range of common ESI instruments (usually *m*/*z* 2000−3000). Instead, it is unequivocally identified by a molecular ion with a charge, which, when divided by the postulated number of polypeptide chains of the oligomer, yields a noninteger number.[21,22] We have recorded the spectrum of the G185R mutant together with the wild-type peptides in TFE for comparison. Several characteristic peaks are summarized in Table 2. For the G185R mutant (MW 2861), the peaks at *m*/*z* 1430.8 and 954.6 are nonspecific. They can be derived from either a monomer or various oligomers, and are not diagnostic. The peaks at *m*/*z* 1073.1 and 537.9, however, are attributable to either a trimer or a hexamer. The presence of a peak at *m*/*z* 748.4 is characteristic of hexameric assembly. Similarly, for the wild-type peptide (MW 2762), both peaks at *m*/*z* 1381.5 and 920.9 are nonspecific, while the peaks at *m*/*z* 592.7 and 519.1 are indicative of either a trimer or a hexamer. However, no other diagnostic peaks for a hexamer were observed for the wild-type DMT1 in TFE, suggesting that the wild-type peptide may form a trimer in TFE.

(19) Lyu, P. C.; Liff, M. I.; Marky, L. A.; Kallenbach, N. R. *Science* **1990**, *250*, 669−673.
(20) Zhong, L.; Johnson W. C., Jr. *Proc. Natl. Acad. Sci. U.S.A.* **1992**, *89*, 4462−4465.
(21) Wendt, H.; Dürr, E.; Thomas, R. M.; Przybylski, M.; Bosshard, H. R. *Protein Sci.* **1995**, *4*, 1563−1570.
(22) Fermandjian, S.; Maroum, R. S.; Amekraz, B.; Jankowski, C. K. *Rapid Commun. Mass Spectrom.* **2001**, *15*, 320−324.

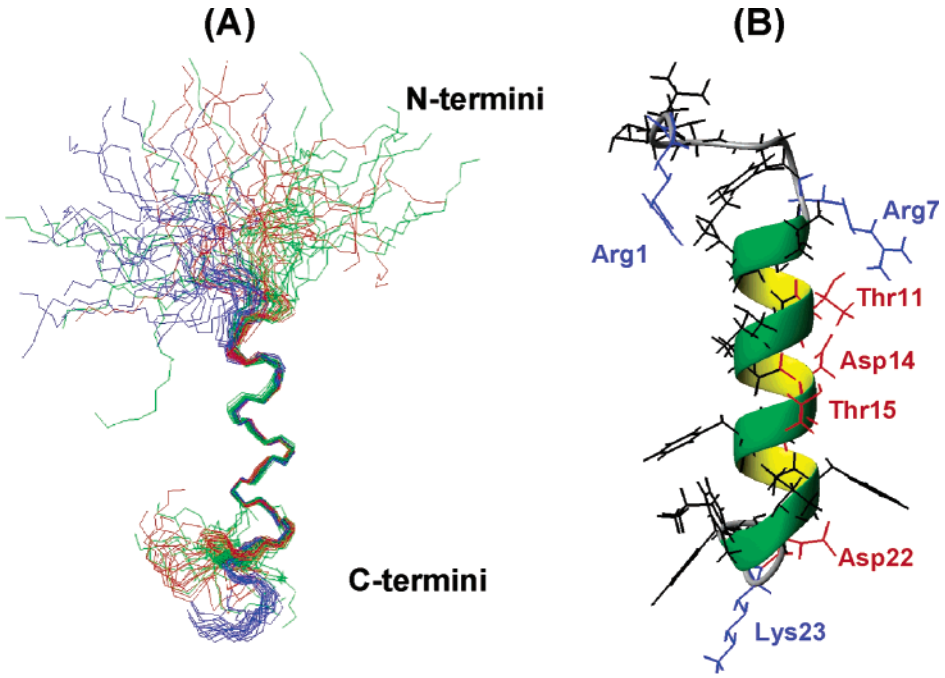


***Figure 4.*** (A) Comparison of the 20 best-converging energy-minimizing structures for the G185R peptide in SDS at pH 4.0 (blue), 6.0 (red), and 7.4 (green). (B) Mean structure of the G185R peptide in SDS micelles at pH 6.0. The side chains are highlighted with stick models. The image was generated using the MOLMOL software.[75] Color code: hydrophilic residues for negatively charged (Asp) and neutral (Thr) residues, red; positively charged residues (e.g., Arg and Lys), blue.

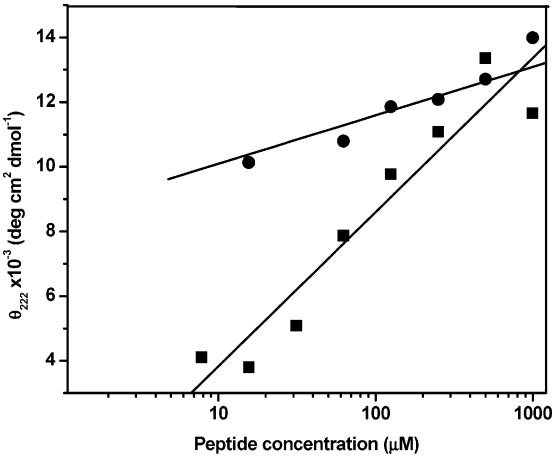


***Figure 5.*** Self-association of the G185R and wild-type peptides: concentration dependence of $\theta_{222}$ for the G185R peptide (●) and wild-type DMT1-TM4 (■) in HFIP, indicative of the presence of different aggregates.

***Table 2.*** . Some Diagnostic Oligomeric Ions Characteristic for Both the G185R Mutant and the Wild-type DMT1-TM4 in TFE and Their Abundances

| relative intensity | G185R mutant | wild type |
|---|---|---|
| high | 1430.8 | 592.7 |
| | 1073.1 | |
| medium | 954.6 | 1381.0 |
| | 537.9 | 920.9 |
| | | 519.1 |
| weak | 748.4 | |

The aggregation of the peptides in TFE was further investigated by diffusion-ordered spectroscopy (DOSY). The translational diffusion coefficient ($D$) is related to the mass of a peptide through the hydrodynamic radius.[23−25] For the wild-type peptide, the DOSY spectrum displays almost a single diffusion coefficient other than the diffusion generated from TFE and impurities (Figure S1 in the Supporting Information). The diffusion coefficient was calculated from the DOSY NMR experiment to be $1.033 \times 10^{-10}$ m$^2$ s$^{-1}$ at 25 °C. In contrast, the DOSY spectrum of the G185R mutant peptide under identical conditions showed at least three diffusion coefficients (Figure S1), suggesting that different peptide components coexist in TFE. The $D$ values corresponding to the three parts from the NH region of the DOSY spectrum are $8.536 \times 10^{-11}$, $1.007 \times 10^{-10}$, and $1.319 \times 10^{-10}$ m$^2$ s$^{-1}$, respectively.

If a prolate ellipsoid model were assumed for the peptide in TFE,[25] the molecular mass for the wild-type peptide would be calculated to be 8.3 kDa, indicative of a trimer of the wild-type peptide in TFE. Similarly, the molecular masses estimated from the diffusion coefficients of the G185R mutant are 14.7, 9.0, and 4.0 kDa, which can be related to a pentamer, trimer, and monomer, respectively. For a peptide with aggregation larger than a trimer, however, the prolate ellipsoid model may not be appropriate. If a sphere model were considered, the molecular mass of the mutant peptide with a diffusion coefficient of $8.536 \times 10^{-11}$ m$^2$ s$^{-1}$ would be 16.2 kDa, corresponding to a hexamer.

Since both the micelle itself and the aggregation of the peptide are probably very flexible, little long-range NOE and interchain H-bonding were observed by NMR, which was also noted in a similar system previously.[26] In addition, the severe overlap in the aliphatic region prevents us from comparing side-chain chemical shifts under different concentrations. Therefore, the self-association of the G185R peptide in SDS micelles was

(23) Dubovskii, P. V.; Dementieva, D. V.; Bocharov, E. V.; Utkin, Y. N.; Arseniev, A. S. *J. Mol. Biol.* **2001**, *305*, 137−149.
(24) Danielsson, J.; Jarvet, J.; Damberg, P.; Gräslund, A. *Magn. Reson. Chem.* **2002**, *40*, S89−S97.
(25) Yao, S.; Howlett, G. J.; Norton, R. S. *J. Biomol. NMR* **2000**, *16*, 109−119.
(26) Damberg, P.; Jarvet, J.; Gräslund, A. *Methods Enzymol.* **2001**, *339*, 271−285.

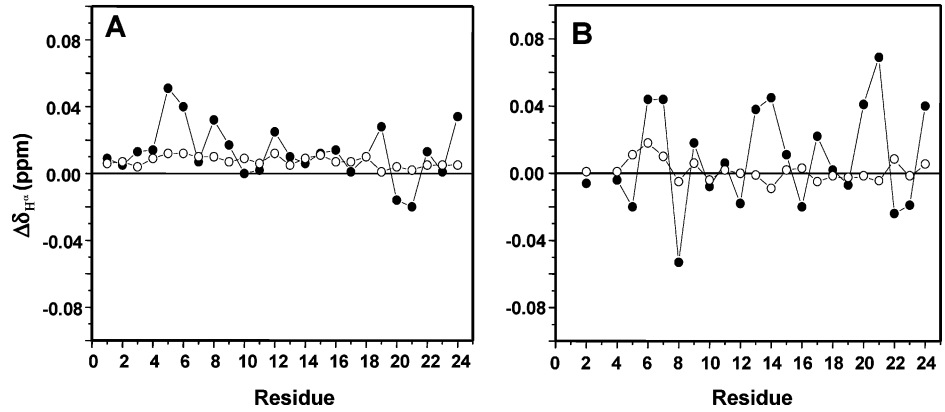


***Figure 6.*** Effects of concentration on chemical shifts of the G185R peptide: (A) $H^\alpha$ and (B) $H^N$ chemical shifts of 0.6 mM peptide in 150 mM SDS-$d_{25}$ (●) and 1 mM peptide in 240 mM SDS-$d_{25}$ (○) relative to those of 2 mM peptide in 300 mM SDS-$d_{25}$.

examined by the effects of concentration and pH on the peptide NMR spectra. The NOESY spectrum (200 ms) of 2 mM G185R peptide in 300 mM SDS-$d_{25}$ at pH 6.0 exhibited relatively good resolution with a reasonable signal-to-noise ratio, which allows assignment of the resonances to be achieved. The intensities of the resonances, particularly in the region of $H^N-H^\alpha$ and $H^N-H^N$, were evidently reduced compared with those for the wild-type DMT1-TM4 peptide under the same conditions.[16] To examine whether this resulted from aggregation, we recorded the NOESY spectra of the G185R peptide at different concentrations (e.g., 0.6 and 1 mM peptide in 150 and 240 mM SDS-$d_{25}$, respectively) at the same pH value (pH 6.0). The peptide at concentrations of 1 and 2 mM gave rise to similar chemical shifts for both $H^\alpha$ and $H^N$, whereas the peptide at a concentration of 0.6 mM exhibited larger differences in both $H^\alpha$ and $H^N$ chemical shifts compared with those obtained at higher peptide concentrations (Figure 6). The chemical shifts of $H^\alpha$ and $H^N$ of the 0.6 mM peptide in 300 mM SDS-$d_{25}$ at pH 6.0 are identical to those in 150 mM SDS-$d_{25}$ (data not shown). Therefore, the changes in chemical shifts for certain residues are probably due to the interactions between different monomers.

The NOESY spectrum of the G185R peptide recorded at pH 4.0 had a notably poorer resolution than those at pH 6.0 and 7.4 under the same conditions (data not shown), although most of the cross-peaks can still be reliably identified at this pH. This suggests that aggregation is favored at a low pH.

**Amide Proton Temperature Coefficients and Solvent Accessibility.** We performed H−D exchange experiments in $D_2O$ at pH* 6.0 and at 25 °C. However, the intensities of the $H^N$ protons in the 1D NMR spectrum decreased by about 70% within 20 min after the peptide/micelle sample was dissolved in $D_2O$. It was therefore impossible to compare amide exchange rates by even a fast 2D NMR method. Extensive signal overlap also prevented the utilization of 1D NMR for measurements of exchange rates.

The effect of temperature on amide proton chemical shifts is a simple but relatively reliable indicator of the strength of the hydrogen bond or shielding from the solvent.[27] A low-temperature coefficient of the amide proton ($\Delta\delta/\Delta T < 2.5$ ppb/K) in an aqueous environment usually indicates the presence of a stable hydrogen bond,[28] while a high-temperature coefficient (e.g., $\Delta\delta/\Delta T > 5$ ppb/K) suggests a solvent-accessible part.[27−29] The temperature coefficients of residues Val2, Leu4, and Tyr5 were larger than 6 ppb/K (data not shown), consistent with the absence of H-bonds. Surprisingly, residues situated in the helical region, which were supposed to have a low value ($\Delta\delta/\Delta T <$ 2.5 ppb/K), had large temperature coefficients (6 ppb/K, data not shown), suggesting a possible solvent accessibility.

**Spin-Label and $Mn^{2+}$ Studies.** The selective broadening of NMR signals of the peptide by paramagnetic probes, including the spin-labels of 5- and 16-doxylstearic acids as well as $Mn^{2+}$ ion, was used to determine the position of the G185R peptide relative to the SDS micelle surface. Two detergent-like spin-labeled compounds, 5- and 16-doxylstearic acids, were readily incorporated into micelles. Radical groups of 5- and 16-DSA were shown close to the micelle surface and near the center of the micelle, respectively.[30] $Mn^{2+}$ has been previously demonstrated as a paramagnetic probe to explore solvent-exposed residues for membrane peptides, since it only broadens the residues situated in the aqueous phase or at the surface of detergent micelles at a low concentration.[31,32] The paramagnetic broadening effects were studied by comparing one- and two-dimensional spectra (NOESY) in the presence and absence of the paramagnetic agents. The amplitudes of the spectra in the presence of paramagnetic agents were normalized to the least affected cross-peaks.

Figure 7 shows the residual relative intensities of the $H^\alpha-H^N$ cross-peaks from NOESY spectra in the presence of paramagnetic agents. Both 5- and 16-doxylstearic acids were added to the peptide samples at SDS:spin-label molar ratios of 60:1, corresponding to approximately one spin-label per micelle. Addition of 16-DSA into the peptide/SDS micelle solution at pH 6.0 resulted in a significant broadening of the $H^\alpha-H^N$ cross-peaks from the hydrophobic residues Leu9, Ile12, Ala13, and Phe16, which completely disappeared from the NOESY spectrum. The intensities of cross-peaks from hydrophilic residues (e.g., Thr11, Asp14, and Thr15), Ile10, and Val17 as well as the N-terminal residues were affected only moderately. In contrast, the addition of 16-DSA hardly affected the cross-peaks of the C-terminal residues (Leu19−Tyr24). Addition of 5-DSA

(27) Cierpicki, T.; Otlewski, J. *J. Biomol. NMR* **2001**, *21*, 249−261.
(28) Hsu, S.-T.; Breukink, E.; de Kruijff, B.; Robert, K.; Bonvin, A. M. J. J.; van Nuland, N. A. J. *Biochemistry* **2002**, *41*, 7670−7676.
(29) Marcinowski, K. J.; Shao, H.; Clang, E. L.; Zagorski, M. G. *J. Am. Chem. Soc.* **1998**, *120*, 11082−11091.
(30) Papavoine, C. H. M.; Konings, R. N. H.; Hilbers, C. W.; van de Ven, F. J. M. *Biochemistry* **1994**, *33*, 12990−12997.
(31) Lindberg, M.; Jarvet, J.; Langel, Ü.; Gräslund, A. *Biochemistry* **2001**, *40*, 3141−3149.
(32) Lindberg, M.; Gräslund, A. *FEBS Lett.* **2001**, *497*, 39−44.

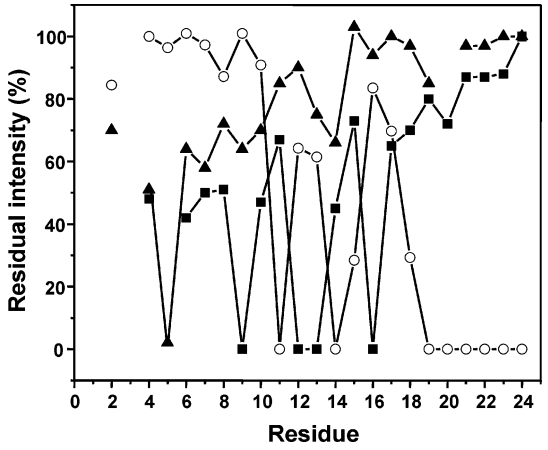


***Figure 7.*** Effects of paramagnetic agents on the NMR signal intensities of the G185R peptide: relative residual intensity of $H^N-H^\alpha$ NOESY cross-peaks of 2 mM G185R peptide in 300 mM SDS-$d_{25}$ in the presence of 5 mM 5-DSA (▲), 5 mM 16-DSA (■), and 0.2 mM $Mn^{2+}$ (○).

into the peptide/SDS micelle solution at pH 6.0 led to marked decreases in intensities for the N-terminal residues, particularly Tyr5, while the cross-peaks of other residues were less affected. The spin-label experiments demonstrated that the peptide was embedded into the interior of SDS micelles at pH 6.0, with the C-terminus exposed outside the micelles.

Addition of 0.2 mM $Mn^{2+}$ to the peptide/SDS micelle solution at pH 6.0 led to the complete disappearance of the cross-peaks of the C-terminal residues from Leu19 to Tyr24 in the 2D NOESY spectrum, indicating that these residues were situated in the aqueous phase, probably outside the micelles. Unexpectedly, $Mn^{2+}$ dramatically decreased the intensities of the cross-peaks from hydrophilic residues Thr11, Asp14, and Thr15, situated in the helical region of the peptide (Figure 7), suggesting a solvent or metal-accessible assembly in the structure. The residues affected markedly upon addition of $Mn^{2+}$ were those least affected in the presence of 16-DSA. The N-terminal residues were almost unaffected in the presence of $Mn^{2+}$, indicating that the N-terminus was also embedded in the SDS micelles. Surprisingly, when the pH of the peptide in the presence of 0.2 mM $Mn^{2+}$ was decreased from 6.0 to 4.0, all the NOESY cross-peaks that disappeared at pH 6.0 recovered promptly (data not shown). When the pH of the sample was raised to 6.0, these signals disappeared again. These experiments demonstrate that the C-terminus may move up or down from the micelles, thereby regulating the entrance of $Mn^{2+}$.

## Discussion

The use of crystallography and NMR techniques should help to elucidate the structural basis of protein function. However, it has been proven to be extremely challenging in the case of membrane proteins because they are notoriously difficult to crystallize. Moreover, integral membrane proteins have slower reorientation rates when complexed with lipids, which limit the application of multidimensional NMR methods. Consequently, less is known about the structures of membrane proteins than those of globular proteins. Recently, model peptides, corresponding to the sequences of potential functional segments or domains of integral proteins, have been demonstrated to be ideal objects for investigation of structure and function in several integral proteins.[33−36]

DMT1 has been found to play an essential role in iron homeostasis. It has been demonstrated that the G185R mutation in the TM4 of DMT1 is a disease-causing mutation in animals, which results in the reduction or loss of the DMT1 function of iron transport.[9] We have previously characterized the structures and topology of a synthetic peptide, corresponding to the fourth transmembrane domain (wild-type DMT1-TM4) in both TFE and SDS micelles by CD and NMR spectroscopies.[15,16] In the present study we examined the three-dimensional structures, assembly, and topology of the G185R peptide, corresponding to the fourth transmembrane domain with the G185R mutation (the G185R peptide), with the aim of establishing a structural basis for elucidating the active mechanism of DMT1. Our results show that the G185R peptide exhibits remarkably similar structures in both TFE and SDS micelles. The structures were characterized by three regions. The N-terminal fragment is in a random coil conformation, which is poorly defined in both TFE and SDS micelles at various pH values. The central part of the peptide exhibits an α-helical conformation in both environments. The C-terminus assumes an α-helical folding in TFE and SDS at pH 4.0, but is disordered in SDS micelles at higher pH values (e.g., 6.0 and 7.4). The calculated structures are consistent with observed NOE connectivities, temperature coefficient data, CSI predictions, and the results of CD experiments. Interestingly, the folding of the C-terminus depends on the pH values: the lower the pH values, the longer the helix formed.

The location of the G185R peptide relative to the SDS micellar surface was studied by using paramagnetic probes, including spin-labeled 5- and 16-doxylstearic acids and a paramagnetic $Mn^{2+}$. This method has been applied previously to determine the orientation of peptides or proteins relative to the surface and interior of detergents.[31,32,37−41] The 16-DSA significantly broadened the cross-peaks of residues Leu9, Ile12, Ala13, and Phe16, but only slightly broadened those of other residues situated in the central part of the peptide in the NOESY spectrum at pH 6.0 (Figure 7). Addition of 5-DSA had no evident effect on the intensity of these residues, indicating the possible formation of a helical core of the peptide which is embedded in the SDS micelles. Unexpectedly, the N-terminus of the peptide was not surface-exposed, but simultaneously was located within the micelles and close to the micelle surface. This is evidenced by the lesser effects of $Mn^{2+}$ on the cross-peaks of these residues (Figure 7). The intensities of the cross-peaks for the C-terminal residues were almost unchanged in the presence of 5-DSA and 16-DSA at pH 6.0 but completely disappeared in the presence of 0.2 mM $Mn^{2+}$, suggesting that the C-terminal residues of the peptide are exposed to aqueous environments. However, the cross-peaks of hydrophilic residues

(33) Opella, S. J.; Marassi, F. M.; Gesell, J. J.; Valente, A. P.; Kim, Y.; Oblatt-Montal, M.; Montal, M. *Nat. Struct. Biol.* **1999**, *6*, 374−379.
(34) MacKenzie, K. R.; Prestegard, J. H.; Engelman, D. M. *Science* **1997**, *276*, 131−133.
(35) Schulz, A.; Bruns, K.; Henklein, P.; Krause, G.; Schubert, M.; Gudermann, T.; Wray, V.; Schultz, G.; Schöneberg, T. *J. Biol. Chem.* **2000**, *275*, 37860−37869.
(36) Ohlenschläger, O.; Hojo, H.; Ramachandran, R.; Görlach, M.; Haris, P. I. *Biophys. J.* **2002**, *82*, 2995−3002.
(37) Brown, L. R.; Bösch, C.; Wüthrich, K. *Biochim. Biophys. Acta* **1981**, *642*, 296−312.
(38) Pellegrini, M.; Bisello, A.; Rosenblatt, M.; Chorev, M.; Mierke, D. F. *Biochemistry* **1998**, *37*, 12737−12743.
(39) Piserchio, A.; Usdin, T.; Mierke, D. F. *J. Biol. Chem.* **2000**, *275*, 27284−27290.
(40) Chang, D.-K.; Cheng, S.-F.; Trivedi, V. D.; Yang, S.-H. *J. Biol. Chem.* **2000**, *275*, 19150−19158.
(41) Wu, J.; So, S. P.; Ruan, K. H. *Arch. Biochem. Biophys.* **2003**, *411*, 27−35.

Thr11 and Asp14 completely disappeared and the cross-peaks of Thr15 broadened significantly at pH 6.0 in the presence of $Mn^{2+}$ (Figure 7), indicating that these residues may be water-accessible. It seems odd that these hydrophilic residues, which are embedded in the SDS interior, are water-accessible. One possible explanation may be that a water-filled channel is formed through self-association of several peptide monomers. The side chains of hydrophilic residues such as Thr11, Asp14, and Thr15 are probably located in the interhelical space of the oligomer to reduce the unfavorable free energy induced by their immersion in hydrophobic environments, while the side chains of Leu9, Ile12, Ala13, and Phe16 reside on the external face of the oligomer to interact with the hydrophobic micelle interior.

When the pH of the G185R peptide was lowered in the presence of 0.2 mM $Mn^{2+}$, the cross-peaks that disappeared at pH 6.0 (including Thr11, Asp14, Thr15, and the C-terminal residues) reappeared. As the peptide does not orientate significantly differently at pH 4.0 compared with pH 6.0, a possible explanation is (in light of our hypothesis of the formation of a channel) that the C-terminal fragment which folds as a helix at pH 4.0 shrinks into the SDS micelles, "blocking" the entrance of $Mn^{2+}$ at this pH value. Therefore, the C-terminus appears to play an important role in the regulation of the metal transport, and further work is needed to determine whether this is also the case for the integral protein.

We observed no obvious difference between the three-dimensional structures and topologies of the G185R peptide and those of the wild-type. Both peptides adopt predominately α-helical structures, embedded in the SDS micelles. The chemical shifts of $H^{\alpha}$ and $H^{N}$ for the G185R peptide are very similar to those for the wild type, except for the residues in the vicinity of Arg7. Our CD, ESI-MS, and NMR data indicated that, despite similarities in the secondary and 3D structures, the quaternary structures of the G185R mutant and the wild-type peptides were different. We observed that the molar residue ellipiticity at 222 nm increased with the increase of the peptide concentrations, but in a different manner for both the G185R mutant and the wild-type peptides (Figure 5).

There is an increasing interest in the use of diffusion measurements to monitor self-aggregation phenomena in proteins and peptides.[23−25] Our diffusion studies by NMR indicated that the wild-type peptide formed a trimer in TFE on the basis of its diffusion coefficient while the G185R peptide showed at least three diffusion coefficient "regions", roughly corresponding to monomer, trimer, and pentamer/hexamer. The uncertainties of the apparent mass of pentamer or hexamer perhaps arise from minor errors or uncertainties of the diffusion coefficient ($D$), viscosity ($\eta$), shape factor ($F$), model used, and possible exchange between trimer and pentamer/hexamer. The ESI-MS data demonstrated that the G185R peptide formed a hexamer in TFE. Therefore, a mixture of a hexamer and a trimer (and other minor forms) may exist for G185R peptide in TFE, on the basis of both the diffusion coefficient measurements and ESI-MS data. Unfortunately, it was not technically possible to perform an ESI-MS study in the SDS micelles. However, distinct differences in the intensities and resolutions of NOESY spectra were observed between the two peptides under the same conditions, suggesting that they may also aggregate differently in the SDS micelles. The wild-type peptide exhibited similar NOESY spectra both at pH 6.0 and at pH 4.0. In contrast, the G185R peptide showed significantly poorer resolution and lower signal-to-noise ratios at pH 4.0 than at pH 6.0, suggesting that the formation of a helix favors an aggregation. These results are consistent with a previous report.[42]

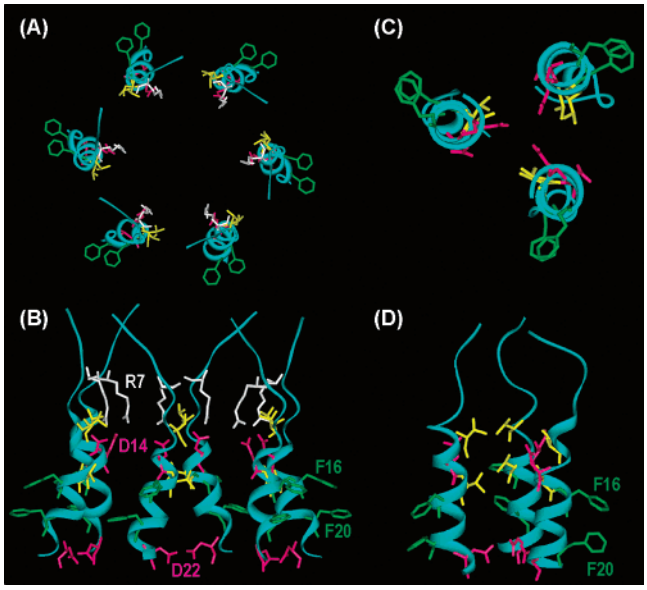


***Figure 8.*** Proposed hexameric and trimeric assemblies for the G185R of TM4 (A, B) and the wild type of TM4 of DMT1 (C, D). The model incorporates results from NMR, ESI-MS, and CD data. Arg7 is highlighted in metallic white, Asp14 and Asp22 are highlighted in purple, Thr11 and Thr15 are highlighted in yellow, and hydrophobic residues Phe16 and Phe20 are highlighted in green. The peptide backbone is highlighted in cyan. Axial and side views are displayed in the top (A, C) and bottom (B, D) panels, respectively. Note in the axial view that the side chains of Arg7 in G185R TM4 are inside the channel. Side chains of hydrophilic residues, e.g., Thr11, Asp14, Thr15, and Asp22, are also inside the channel, whereas side chains of Phe16 and Phe20 are probably exposed to the hydrophobic phase. The modeling was performed by using CHARMm, and the diagrams were generated by ViewerLite.

Membrane peptides can assume functional assembly just like their integral proteins, even in detergent micelles.[33,43,44] On the basis of our studies of both the G185R mutant and the wild-type peptides, we hypothesize that the integral DMT1 may function as a divalent metal channel either by self-assembly of several monomers, such as the potassium ($K^+$)[45] and chloride ($Cl^-$) channels,[46] or by organization of several homologous domains, such as sodium ($Na^+$) channels.[47] A hexameric assembly for G185R TM4 was proposed by molecular modeling. The trimeric assembly for the wild type of TM4 of DMT1 was also shown for comparison, Figure 8. The two glycine residues located within the putative transmembrane domain 4 of DMT1 are conserved among the Nramp family proteins, and seem to be particularly important for the function of its integral protein. Indeed, both disease-causing mutations in the Nramp family proteins occurred at these two Gly residues.[7,48] It has been noticed that large proportions of glycine residues are often

(42) Chang, D. K.; Cheng, S. F.; Trivedi, V. D. *Arch. Biochem. Biophys.* **2001**, *396*, 89−98.
(43) Tang, P.; Mandal, P. K.; Xu, Y. *Biophys. J.* **2002**, *83*, 252−262.
(44) Chia, C. S. B.; Torres, J.; Copper, M. A.; Arkin, I. T.; Bowie, J. H. *FEBS Lett.* **2002**, *512*, 47−51.
(45) Doyle, D. A.; Cabral, J. M.; Pfuetzner, R. A.; Kuo, A.; Gulbis, J. M.; Cohen, S. L.; Chait, B. T.; MacKinnon, R. *Science* **1998**, *280*, 69−77.
(46) Dutzler, R.; Campbell, E. B.; Cadene, M.; Chait, B. T.; MacKinnon, R. *Nature* **2002**, *415*, 287−294.
(47) Favre, I.; Moczydlowski, E.; Schild, L. *Biophys. J.* **1996**, *71*, 3110−3125.
(48) Vidal, S. M.; Malo, D.; Vogan, K.; Skamene, E.; Gros, P. *Cell* **1993**, *73*, 469−485.

present in the putative TM domains of integral membrane proteins. The main role of these glycine residues appears to provide a small side chain for packing interaction, rather than to impart characteristics of flexibility normally associated with this residue.[49,50] The substitution of a small and uncharged glycine (Gly185) by the bulky and positively charged arginine (Arg7) alters the assembly of TM4 from a trimer in the wild type to a hexamer and may disrupt the quaternary structure or the self-assembly of the intact DMT1 in vivo. The polar residues have been shown previously to promote helix association through the formation of side-chain/side-chain interhelical hydrogen bonds in detergent micelles and in biological membranes.[51,52] For example, the G708N in the transmembrane helix of the $\beta$3 subunit of integrin $\alpha$2||b$\beta$3 enhances the tendency of the transmembrane helix to form homotrimers, and this mutation also enhances the activation of the integral protein.[53] Our ESI-MS and diffusion coefficient data indeed suggest that the mutation of glycine to arginine (corresponding to Gly185 → Arg185) enhances such a helix association, possibly from a trimer to a hexamer. Therefore, the possible changes in the quaternary structure of DMT1 may help to explain why a missense mutation (G185R) abolishes the function of DMT1. Further experiments are required to investigate whether other mechanisms may also be involved.

In summary, we have provided the first structural and topological survey of the fourth transmembrane domain of a disease-causing mutation (G185R) in membrane-mimetic environments, i.e., TFE and SDS micelles. The G185R peptide exhibits three-dimensional structures extremely similar to that of the wild type, and has a similar topology. The disordered N-terminus and a well-defined central helical segment are embedded into the interior of the SDS micelles, and interestingly, both the folding and location of the C-terminus are triggered by pH values. Unexpectedly, the G185R peptide exhibits a self-assembly distinct from that of the wild type (Figures 5 and 8). The findings suggest that integral DMT1 might transport divalent metal ions via formation of a channel through either self-association or arrangement of its transmembrane domains, while substitution of the Gly185 by a bulky and positively charged Arg probably alters its quaternary structure, which in turn abolishes its function.

## Experimental Section

**Materials.** The peptide with a sequence of RVPLYG*R*VLITIADT-FVFLFLDKY-OH, corresponding to the transmembrane domain 4 of rat DMT1 (179−202) with G185R mutated, was produced by solid-phase synthesis and purified by HPLC on a Zorbax SB phenyl reversed-phase column using 0.1% TFA/water and 0.1% TFA/acetonitrile as solvents (Biopeptide Co., LLC). Peptide purity was assessed by HPLC and mass spectroscopy to be above 95%. Deuterated sodium dodecyl sulfate (SDS-$d_{25}$; 98%) and deuterated 2,2,2-trifluoroethanol (TFE-$d_2$; 98%) were purchased from Cambridge Isotope Laboratories. Trifluoroacetic acid (TFA; 99%), 5- and 16-doxylstearic acids (5-DSA and 16-DSA), 1,1,1,3,3,3-hexafluoro-2-propanol (HFIP), sodium dodecyl sulfate (SDS), and DEWX 50 WXZ-200 (H) resin were obtained from Sigma. 2,2,2-Trifluoroethanol (TFE; 99.8%) was purchased from Acros Organics. All chemicals were used as purchased, without further treatment.

**Sample Preparation.** For CD experiments, the peptide was either directly dissolved in organic solvents (TFE or HFIP) to produce different concentrations of peptide or incorporated into SDS micelles as described previously.[54] A 12 $\mu$L sample of peptide stock solution (0.5 mM peptide in HFIP) was added to 12 $\mu$L of SDS stock solution (250 mM SDS in $H_2O$), the resulting solution was vortexed for 2 s, and $H_2O$ was added to the mixture to yield a 16:1 ratio of water to SDS by volume. The mixture was lyophilized overnight, and the resulting powder was rehydrated in 300 $\mu$L of water. The pH was adjusted to desired values.

For NMR experiments, ca. 4 mg of the peptide was dissolved in 0.6 mL of TFE-$d_2$. The insoluble part was removed by low-speed centrifugation. Similarly as described above, 3.2 mg of the peptide was dissolved in 200 $\mu$L of HFIP and mixed with 56.4 mg of SDS-$d_{25}$ solubilized in 200 $\mu$L of $H_2O$. The mixture was further diluted by the addition of 1.6 mL of $H_2O$ and lyophilized overnight. The resulting powder was dissolved in 0.6 mL of a $H_2O/D_2O$ (90%/10%) mixture in a 5 mm sample tube. The pH was adjusted by the addition of a small amount of NaOH or HCl solution.

**Circular Dichroism Spectropolarimetry.** Far-UV CD spectroscopy was performed at room temperature on a Jasco J-720 spectropolarimeter, using a quartz cuvette with a path length of 0.1 or 1 mm. The data were recorded between 190 and 260 nm in a step of 0.1 nm, with a scan speed of 50 nm/min. Four scans were averaged for each spectrum, and the reference spectra of the respective media were subtracted. Molar ellipticity values were calculated according to the equation $[\theta] = \theta/(10lcn)$, where $\theta$ is the ellipticity in millidegrees, $l$ is the path length in centimeters, $c$ is the molar concentration of the peptide, and $n$ is the number of amino acid residues of the peptide. The helix content was estimated using the program CONTINLL[55,56] from the CDPro software package.[57]

**NMR Spectroscopy.** All spectra were recorded on a Bruker AV 600 spectrometer. The homonuclear two-dimensional TOCSY[58,59] and NOESY spectra[60,61] were obtained at 25 °C using the WATERGATE technique for water suppression.[62] The TOCSY spectra employed the MLEV-17-spin-lock,[63] with mixing times of 50−100 ms. The NOESY experiments were recorded at a series of mixing times (50, 100, 200, and 250 ms). The data were acquired with 2048 complex points in the direct dimension, and 512 data points in the indirect dimension. The States-TPPI method[64] was used for quadrature detection in $t_1$. The proton chemical shifts were referenced to sodium salt of 3-(trimethylsilyl)-propionate-2,2,3,3-$d_4$.

The NMR spectra were processed using the XWINNMR software (version 3.1), zero-filled to 2048 × 2048 matrices, and apodized by a squared sine bell window function prior to Fourier transformation.

The H−D exchange experiments were performed using 2 mM peptide incorporated into 300 mM SDS-$d_{25}$ in $D_2O$ at 25 °C and pH* 6.0. For measurements of the temperature coefficient of amide protons, the NOESY spectra of 2 mM peptide in 300 mM SDS-$d_{25}$ were recorded from 15 to 40 °C in steps of 5 °C. The temperature coefficients ($-\Delta\delta$/

(49) Jung, K.; Jung, H.; Colacuricio, P.; Kaback, H. R. *Biochemistry* **1995**, *269*, 1030−1039.
(50) Loo, T. W. *J. Biol. Chem.* **1994**, *269*, 7243−7248.
(51) Zhou, F. X.; Merianos, H. J.; Brunger, A. T.; Engelman, D. M. *Proc. Natl. Acad. Sci. U.S.A.* **2001**, *98*, 2250−2255.
(52) Dawson, J. P.; Melnyk, R. A.; Deber, C. M.; Engelman, D. M. *J. Mol. Biol.* **2003**, *331*, 255−262.
(53) Li, R.; Mitra, N.; Gratkowski, N.; Vilaire, G.; Litvinov, R.; Nagasami, C.; Weisel, J. W.; Lear, J. D.; DeGrado, W. F.; Bennett, J. S. *Science* **2003**, *300*, 795−798.
(54) Killian, J. A.; Trouard, T. P.; Greathouse, D. V.; Chupin, V.; Lindblom, G. *FEBS Lett.* **1994**, *348*, 161−165.
(55) Provencher, S. W.; Glockner, J. *Biochemistry* **1981**, *20*, 33−37.
(56) van Stokkum, I. H.; Spoelder, H. J.; Bloemendal, M.; van Grondelle, R.; Groen, F. C. *Anal. Biochem.* **1990**, *191*, 110−118.
(57) Sreerama, N.; Woody, R. W. *Anal. Biochem.* **2000**, *287*, 252−260.
(58) Braunschweiler, L.; Ernst, R. R. *J. Magn. Reson.* **1983**, *53*, 521−528.
(59) Bax, A.; Davis, D. G. *J. Magn. Reson.* **1985**, *65*, 355−360.
(60) Jeener, J.; Meier, B. H.; Bachmann, P.; Ernst, R. R. *J. Chem. Phys.* **1979**, *71*, 4546−4553.
(61) Kumar, A.; Wagner, G.; Ernst, R. R.; Wüthrich, K. *J. Am. Chem. Soc.* **1981**, *103*, 3654−3658.
(62) Piotto, M.; Saudek, V.; Sklenar, V. *J. Biomol. NMR* **1992**, *2*, 661−666.
(63) Levitt, M. H.; Freeman, R.; Frenkiel, T. *J. Magn. Reson.* **1982**, *47*, 328−330.
(64) Marion, D.; Wüthrich, K. *Biochem. Biophys. Res. Commun.* **1983**, *113*, 967−974.

$\Delta T$, ppb/K) were taken from the slopes of the least-squares fitted lines of the chemical shifts $\delta_H^N$ vs temperatures.

Diffusion coefficient measurements were performed on a Bruker DRX 500 MHz spectrometer equipped with a *z*-axis gradient coil. All spectra were acquired in a 5 mm TBI probehead at 25 °C in 5 mm sample tubes. The gradient strength was calibrated using the HDO signal in $D_2O$.[65] The stimulated echo bipolar pulse sequence using WATERGATE for water suppression was applied to DOSY experiments with a diffusion time ($\Delta$) of 250 ms in all experiments. The durations of the gradient pulse ($\delta$) were 4.6 and 4.0 ms for the wild-type and G185R mutated peptides, respectively, to obtain a 1−5% residual signal with the maximum gradient strength. The pulse gradients ($g$) were incremented from 2% to 95% of the maximum gradient strength in a linear lamp, and the data were acquired with 8−64 transients. After Fourier transformation and baseline correction, the diffusion dimension was processed with the two-exponential decays using the XWINNMR software.

**Paramagnetic Broadening Experiments.** Samples of 2 mM peptide in 300 mM SDS-$d_{25}$ were used in these experiments. Freshly prepared spin-labels (5- or 16-DSA), solubilized in a small volume of methanol-$d_4$, were added to the peptide at pH 6.0 to yield a final concentration of 5 mM. (On the assumption of 60 molecules in each SDS micelle, this corresponded to one spin-label per micelle.) NOESY spectra in the absence and presence of the spin-labels were recorded under identical conditions. Similarly, $MnCl_2$ was added to the peptide at final concentrations of 0.1 and 0.2 mM. The NOESY spectra were recorded again. The amplitudes of the spectra in the presence of the paramagnetic agents were normalized to the least affected cross-peaks.

**Electrospray Ionization Mass Spectrometry.** ESI-MS spectra were recorded using an unmodified LCQ spectrometer (Finnigan Corp.) with a working *m*/*z* range of 500−2000, in a positive ion mode. The peptides (both the wild type and the G185R mutant) were dissolved in TFE, producing a concentration of ca. 0.3 mM. The peptides were treated with DEWX 50 WXZ-200 (H) resin, which was pretreated with 0.5% HCl and washed thoroughly to remove any trace amount of sodium. The peptide solutions were infused at 3 $\mu$L·min$^{-1}$. Working conditions used were as described previously.[22] The source temperature was 453−473 K, and the drying gas flow rate was 0.9 L·min$^{-1}$. Potentials of 3.5 and 5−30 kV were applied to the probe tip and cone, respectively. The quadruple was scanned at 100 amu·s$^{-1}$. The mass accuracy of all measurements was within 0.5 *m*/*z* unit.

**Structure Calculation.** The structural calculation of the G185R peptide was carried out with the program CYANA (1.0).[66] Distance constraints were derived from NOESY spectra recorded with a mixing time of 200 ms. No dihedral angle constraints were used in the structural calculations since backbone amide peaks were too broad. NOE intensities and chemical shifts were extracted using the Sparky software,[67] and served as an input for the CYANA program. Integrals were transformed into upper distance bounds with the macro CALIBA.[68] The distance constraints were then subjected to a local conformational analysis with the GRIDSEARCH algorithm.[69] Torsion angle dynamic calculations were performed by the macro ANNEAL in the CYANA program. Calculations started from 500 initial random structures, and structures with no violations >0.2 Å for distance constraints and >5.0° for angle constraints were accepted. The 30 structures with the lowest target functions were chosen for further energy minimization under the Cornell et al. 1994 force field,[70] using a generalized Born solvent model[71] in AMBER7,[72,73] The quality of the final 20 best-converging energy-minimizing structures was evaluated using the PROCHECK-NMR program.[74] Structural generation and analysis were performed with the MOLMOL program.[75]

**Calculation of Apparent Molecular Mass from the Translational Diffusion Coefficient.** The following equation was used to estimate the molecular mass ($M$) on the basis of the diffusion coefficient ($D$) assuming the peptides to be a prolate ellipsoid in TFE:[25]

$$M = (k_B T/6\pi\eta F D)^3 [4\pi N_A/[3(\nu_2 + \delta_1 \nu_1)]] \quad (1)$$

where $k_B$ is the Boltzmann constant, $T$ is the absolute temperature (K), $\eta$ is the viscosity of the solution ($1.35 \times 10^{-3}$ N s m$^{-2}$ for the peptide/TFE solution[76]), $N_A$ is Avogadro's number, $\nu_1$ and $\nu_2$ are the specific volumes of the solvent molecule and the peptides, respectively ($7.2 \times 10^{-4}$ and $7.7 \times 10^{-4}$ m$^3$ kg$^{-1}$ based on the amino acid composition[24,77]), and $\delta_1$ is the fractional amount of TFE bound to the peptide, and a value of 0.4 was used under the conditions used.[25] A shape factor ($F$) of 1.0325 was used for a prolate ellipsoid with an axial ratio of 0.55 for the peptide in TFE.[25]

**Acknowledgment.** This work is supported by the University Grants Committee (Hong Kong) under the Scheme of the Area of Excellence, Hong Kong Research Grants Council (Grant HKU 7227/02M to Q.-Y.H.) and the University of Hong Kong (Grant URC to H.S. and Q.-Y.H.). We are grateful for an equipment grant (large item of equipment) from the University of Hong Kong for the purchase of a 600 MHz NMR spectrometer. We thank Mr. S. C. Yan for assistance in the ESI-MS experiments.

**Supporting Information Available:** Figure showing the DOSY spectra of the wild-type and G185R mutant peptides (PDF). This material is available free of charge via the Internet at http://pubs.acs.org.

JA047148T

(65) Mills, R. *J. Phys. Chem.* **1973**, *77*, 685−688.
(66) Güntert, P.; Mumenthaler, C.; Wüthrich, K. *J. Mol. Biol.* **1997**, *273*, 283−298.
(67) Goddard, T. D.; Kneller, D. G. University of California, San Francisco, 2001.
(68) Güntert, P.; Braun, W.; Wüthrich, K. *J. Mol. Biol.* **1991**, *217*, 517−530.
(69) Güntert, P.; Billeter, M.; Ohlenschläger, O.; Brown, L. R.; Wüthrich, K. *J. Biomol. NMR* **1998**, *12*, 543−548.
(70) Cornell, W. D.; Cieplak, P.; Bayly, C. I.; Gould, I, R.; Merz, K. M.; Ferguson, D. M., Jr.; Spellmeyer, D. C.; Fox, T.; Caldwell, J. W.; Kollman, P. A. *J. Am. Chem. Soc.* **1995**, *117*, 5179−5197.
(71) Tsui, V.; Case, D. A. *Biopolymers (Nucleic Acid Sci.)* **2001**, *56*, 275−291.
(72) Pearlman, D. A.; Case, D. A.; Caldwell, J. W.; Ross, W. S.; Cheatham, T. E.; DeBolt, S.; Ferguson, D.; Seibel, G.; Kollman, P. *Comput. Phys. Commun.* **1995**, *91*, 1−41.
(73) Case, D. A.; Pearlman, D. A.; Caldwell, J. W.; Cheatham, T. E., III; Wang, J.; Ross, W. S.; Simmerling, C. L.; Darden, T. A.; Merz, K. M.; Stanton, R. V.; Cheung, A. I.; Vincent, J. J.; Crowley, M.; Tsui, V.; Gohike, H.; Radmer, R. J.; Duan, Y.; Pitera, J.; Massova, I.; Seibel, G. L.; Singh, U. C.; Weiner, P. K.; Kollman, P. A. University of California, San Francisco, 2002.
(74) Laskowski, R. A.; Rullmann, J. A.; MacArthur, M. W.; Kaptein, R.; Thornton, J. M. *J. Biomol. NMR* **1996**, *8*, 477−486.
(75) Koradi, R.; Billeter, M.; Wüthrich, K. *J. Mol. Graphics* **1996**, *14*, 51−55.
(76) Fioroni, M.; Diaz, M. D.; Burger, K.; Berger, S. *J. Am. Chem. Soc.* **2002**, *124*, 7737−7744.
(77) Perkins, S. J. *Eur. J. Biochem.* **1986**, *157*, 169−180.